



**HAL**  
open science

**Microstructure and electrical properties of  
(Ba<sub>0.6</sub>Sr<sub>0.4</sub>)<sub>0.85</sub>Bi<sub>0.1</sub>TiO<sub>3</sub> ceramics prepared by  
single-step, liquid-phase, solid-state reactive sintering**

Nahum Masó, Cécile Marcelot, Laétitia Fabre, Jean-Baptiste Fruhauf, Pascal Dufour, Christophe Tenailleau, Bénédicte Warot-Fonrose, Etienne Snoeck, Sophie Guillemet-Fritsch

► **To cite this version:**

Nahum Masó, Cécile Marcelot, Laétitia Fabre, Jean-Baptiste Fruhauf, Pascal Dufour, et al.. Microstructure and electrical properties of (Ba<sub>0.6</sub>Sr<sub>0.4</sub>)<sub>0.85</sub>Bi<sub>0.1</sub>TiO<sub>3</sub> ceramics prepared by single-step, liquid-phase, solid-state reactive sintering. *Journal of Electroceramics*, 2018, 40 (3), pp.197-202. 10.1007/s10832-018-0120-7 . hal-01848806

**HAL Id: hal-01848806**

**<https://hal.science/hal-01848806v1>**

Submitted on 28 Oct 2019

**HAL** is a multi-disciplinary open access archive for the deposit and dissemination of scientific research documents, whether they are published or not. The documents may come from teaching and research institutions in France or abroad, or from public or private research centers.

L'archive ouverte pluridisciplinaire **HAL**, est destinée au dépôt et à la diffusion de documents scientifiques de niveau recherche, publiés ou non, émanant des établissements d'enseignement et de recherche français ou étrangers, des laboratoires publics ou privés.



## Open Archive Toulouse Archive Ouverte (OATAO)

OATAO is an open access repository that collects the work of Toulouse researchers and makes it freely available over the web where possible

This is an author's version published in: <http://oatao.univ-toulouse.fr/24527>

**Official URL:** <https://doi.org/10.1007/s10832-018-0120-7>

### To cite this version:

Masó, Nahum  and Marcelot, Cecile and Fabre, Laëtitia and Fruhauf, Jean-Baptiste and Dufour, Pascal  and Tenailleau, Christophe  and Warot-Fonrose, Bénédicte and Snoeck, Etienne and Guillemet, Sophie  *Microstructure and electrical properties of (Ba<sub>0.6</sub>Sr<sub>0.4</sub>)<sub>0.85</sub>Bi<sub>0.1</sub>TiO<sub>3</sub> ceramics prepared by single-step, liquid-phase, solid-state reactive sintering.* (2018) *Journal of Electroceramics*, 40 (3). 197-202. ISSN 1385-3449

Any correspondence concerning this service should be sent to the repository administrator: [tech-oatao@listes-diff.inp-toulouse.fr](mailto:tech-oatao@listes-diff.inp-toulouse.fr)

# Microstructure and electrical properties of $(\text{Ba}_{0.6}\text{Sr}_{0.4})_{0.85}\text{Bi}_{0.1}\text{TiO}_3$ ceramics prepared by single-step, liquid-phase, solid-state reactive sintering

Nahum Masó<sup>1</sup>  · Cecile Marcelot<sup>2</sup> · Laëtitia Fabre<sup>3</sup> · Jean-Baptiste Fruhauf<sup>3</sup> · Pascal Dufour<sup>1</sup> · Christophe Tenailleau<sup>1</sup> · Bénédicte Warot-Fonrose<sup>2</sup> · Etienne Snoeck<sup>2</sup> · Sophie Guillemet-Fritsch<sup>1</sup>

## Abstract

$(\text{Ba}_{0.6}\text{Sr}_{0.4})_{0.85}\text{Bi}_{0.1}\text{TiO}_3$  ceramics have been obtained by single-step, liquid-phase, solid-state reactive sintering in the temperature range 1250–1350 °C using stoichiometric amounts of  $\text{BaTiO}_3$ ,  $\text{SrTiO}_3$  and  $\text{Bi}_4\text{Ti}_3\text{O}_{12}$ . Their microstructure and electrical properties have been studied by X-Ray diffraction and fluorescence, scanning and transmission electron microscopy and impedance spectroscopy. The relative density,  $D_r$ , relative permittivity,  $\epsilon_r'$ , and dissipation factor,  $\tan \delta$ , at room temperature and the bulk and grain boundary resistivity,  $R_b$  and  $R_{gb}$ , and activation energies,  $E_a^b$  and  $E_{gb}^{sb}$ , are approximately independent of the sintering temperature with values around e.g.  $D_r \sim 97.5\%$ ,  $\epsilon_r' \sim 1790$ ,  $\tan \delta \sim 0.06\%$ ,  $R_b^{500^\circ\text{C}} \sim 26 \text{ k}\Omega \text{ cm}$ ,  $E_a^{sb} \sim 1.03 \text{ eV}$ ,  $R_{gb}^{500^\circ\text{C}} \sim 217 \text{ k}\Omega \text{ cm}$  and  $E_a^{gb} \sim 1.41 \text{ eV}$ . By contrast, the temperature coefficient of capacitance, TCC, increases linearly from  $\sim 10 \text{ ppm } ^\circ\text{C}^{-1}$  to  $\sim 21 \text{ ppm } ^\circ\text{C}^{-1}$  on increasing sintering temperature. Comments on the influence of the sintering temperature on the chemical composition of the ceramics are made.

**Keywords** Liquid-phase · Solid-state reactive sintering · Electrical properties ·  $(\text{Ba}_{0.6}\text{Sr}_{0.4})_{0.85}\text{Bi}_{0.1}\text{TiO}_3$  ceramics

## 1 Introduction

Barium titanate,  $\text{BaTiO}_3$ , and strontium titanate,  $\text{SrTiO}_3$ , are the parent materials for a range of commercial electroceramic devices. They form a continuous solid solution [1, 2] with general formula  $\text{Ba}_{1-x}\text{Sr}_x\text{TiO}_3$ ;  $0 \leq x \leq 1$ . On increasing  $x$ , the crystal structure at room temperature changes from tetragonal to cubic at  $x \approx 0.30$ ; the temperatures of rhombohedral-orthorhombic, orthorhombic-tetragonal and tetragonal-cubic

phase transitions of  $\text{BaTiO}_3$  decrease linearly and coalesce at  $x \approx 0.80$  to give a single transition with  $T_{\text{max}}$  at  $\sim 115 \text{ K}$ ; a relaxor behaviour is observed on further increasing  $x$ ; [Refs 3–7] and, finally,  $\text{SrTiO}_3$  is regarded as a quantum paraelectric.

In addition,  $\text{Ba}_{1-x}\text{Sr}_x\text{TiO}_3$  ceramics may also contain a wide variety of dopants in order to further control the temperature of the maximum of the permittivity vs. temperature profile as well as the temperature coefficient of capacitance. In particular, in Bi-doped  $\text{Ba}_{1-x}\text{Sr}_x\text{TiO}_3$  ceramics, a relaxor behaviour near room temperature is observed for low Sr and Bi content, i.e.  $(\text{Ba}_{1-x}\text{Sr}_x)_{1-1.5y}\text{Bi}_y\text{TiO}_3$  with  $0.20 \leq x \leq 0.40$  and  $y \leq 0.10$  [Refs 8–13].

Commonly,  $\text{Ba}_{1-x}\text{Sr}_x\text{TiO}_3$  ceramics are obtained in a two-step process which involves, first, decarbonation and initial reaction of the raw powder reactants, i.e.  $\text{BaCO}_3$ ,  $\text{SrCO}_3$  and  $\text{TiO}_2$ , at low temperature, e.g.  $\sim 1000 \text{ }^\circ\text{C}$ , and, next, sintering of the ceramic body at temperature above e.g.  $\sim 1300 \text{ }^\circ\text{C}$ . In addition, sintering agents, e.g.  $\text{SiO}_2$ , or an excess of one of the reactant, e.g.  $\text{TiO}_2$ , are also added into the formulation since they promote the formation of a liquid phase which enhances the reaction and grain growth during sintering. The use of a liquid phase during sintering is regarded in the literature as

✉ Jean Baptiste Fruhauf  
jbfuhauf@sct\_ceramics.com

✉ Sophie Guillemet Fritsch  
guillem@chimie.ups\_tlse.fr

<sup>1</sup> CIRIMAT, Université de Toulouse, CNRS, INPT, UPS, Université Toulouse 3 Paul Sabatier, Bât. CIRIMAT, 118 route de Narbonne, 31062 Toulouse Cedex 9, France

<sup>2</sup> CEMES CNRS, 29 rue Jeanne Marvig, BP 94347, 31055 Toulouse Cedex 4, France

<sup>3</sup> SCT Société des Céramiques Techniques, ZI Ouest Route d'Oursbelille, BP 9, 65460 Bazet, France

Liquid-Phase Sintering [14] (LPS) or Solid-State Reactive Sintering [15] (SSRS).

The company SCT (Société des Céramiques Techniques) is interested on manufacturing  $(\text{Ba}_{0.6}\text{Sr}_{0.4})_{0.85}\text{Bi}_{0.1}\text{TiO}_3$  ceramics capacitors in a single-step, reproducible approach. In order to do so, we have used the LPS/SSRS approach taking advantage of the low melting temperature of  $\text{Bi}_4\text{Ti}_3\text{O}_{12}$ . The influence of the sintering temperature on the chemical composition, microstructure and electrical properties are reported here.

## 2 Experimental

The starting raw material was a granulated  $(\text{Ba}_{0.6}\text{Sr}_{0.4})_{0.85}\text{Bi}_{0.1}\text{TiO}_3$  powder provided by Ferro. The powder was first dispersed in Darvan C. Then, 1 wt.% PEG 4000 and 2 wt.% Poval 205C were added and the resultant solution was atomised at 315 °C. After powder conditioning, pellets were fabricated by uniaxial compaction at 600 bar of pressure, repressed isostatically at 1000 bar, placed on a bed of sacrificial powder (MgO doped  $\text{ZrO}_2$ ) and sintered in air at several temperatures as follows: 1150 °C for 6 h; 1250 °C, 1300 °C and 1350 °C for 2 h. After sintering, the edge and the faces of the pellets were polished ~0.05 mm and ~0.30 mm, respectively, in order to remove any contamination from the sacrificial powder and/or furnace. The final dimensions of the pellets were 4.75–5.15 mm thick and 20.00–20.20 mm diameter. For statistical purposes, three pellets were characterised for each sintering temperature.

The density of the pellets was determined by the Archimedes method, using water as the immersion liquid. Pellets were first dried at 180 °C overnight, then cooled down to room temperature into a desiccator under vacuum before the density measurement.

Samples were analyzed by X-ray powder diffraction (XRD) at room temperature using a Bruker D4 Diffractometer  $\text{CuK}\alpha$  radiation. Lattice parameters were determined by Le Bail method for reflections in the range  $2\theta < 100^\circ$  using the software GSAS. X-Ray Fluorescence (XRF) used a Bruker S2 Ranger.

For dilatometry, a pellet, ~10 mm thick and ~6 mm diameter, was heated at 1400 °C in air, ~20  $\text{cm}^3 \text{min}^{-1}$ , at 2 °C  $\text{min}^{-1}$  in a Setaram Setsys Evolution 16/18. For thermogravimetry (TG), ~100 mg of powder were heated at 1400 °C in air, ~100  $\text{cm}^3 \text{min}^{-1}$ , at 2 °C  $\text{min}^{-1}$  in a Netzsch STA 409 C thermobalance.

Scanning electron microscopy (SEM) and transmission electron microscopy (TEM) were performed with a JEOL JSM6510LV and FEI CM20, respectively, both equipped with Oxford EDS detectors.

Dielectric and impedance data were collected with an Agilent 4294A impedance analyser over the frequency range 40 Hz to 1 MHz, with an *ac* measuring voltage of 100–500 mV and over the temperature range –60 °C to 650 °C on heating and cooling cycles. For dielectric measurements pellets ~5 mm thick and ~20 mm diameter were analysed whereas impedance measurements used slabs of ~1 to 2.5 mm thick and ~100  $\text{mm}^2$  of area which were obtained by cutting the pellets perpendicularly to both faces. Electrodes were fabricated with Ag paint that was annealed at 760 °C. Data were corrected for the overall pellet geometry and, consequently, resistivity and permittivity data are reported in units of  $\Omega \text{cm}$  and  $\text{F cm}^{-1}$ , respectively.

## 3 Results and discussion

Figure 1(a) shows the mass loss of the green powder and the linear contraction of a green pellet as a function of temperature. Between room temperature and ~400 °C, a weight loss of ~4 % occurred which was associated with evaporation of water and combustion of organic matter, i.e. binders. Between ~700 °C and ~1050 °C, no noticeable weight loss was observed whereas, above ~1050 °C, weight loss occurred gradually and became pronounced above ~1250 °C. No shrinkage was observed up to ~900 °C whereas, above ~900 °C, it became pronounced over the temperature range ~1075–1250 °C. An expansion was finally observed above ~1300 °C.

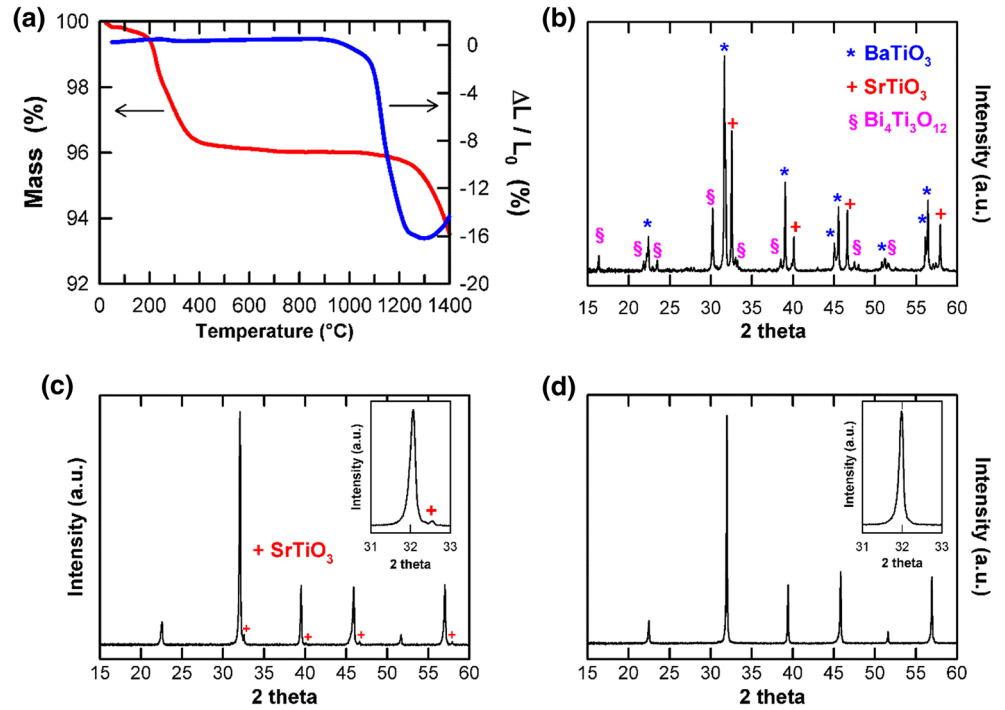
XRD performed on the raw powder of  $(\text{Ba}_{0.6}\text{Sr}_{0.4})_{0.85}\text{Bi}_{0.1}\text{TiO}_3$  used to prepare the ceramics contained a mixture of  $\text{BaTiO}_3$ ,  $\text{SrTiO}_3$  and  $\text{Bi}_4\text{Ti}_3\text{O}_{12}$ , Fig. 1(b). After sintering in the temperature range from 1250 °C to 1350 °C, ceramics were phase pure  $(\text{Ba,Sr,Bi})\text{TiO}_3$  whereas those sintered at 1150 °C contained, in addition to the main phase  $(\text{Ba,Sr,Bi})\text{TiO}_3$ , a small amount of unreacted  $\text{SrTiO}_3$ , Fig. 1(c) and (d). Hereafter, we focus on the phase-pure samples determined by XRD.

Lattice parameters were  $a \approx 3.961(1) \text{ \AA}$  and  $V \approx 62.15(1) \text{ \AA}^3$  in agreement with the literature data [12]. The calculated theoretical density was ~5.79  $\text{g cm}^{-3}$ . The relative density of the pellets (Table 1) decreased from ~98.1(2) % to ~96.9(3) % on increasing the sintering temperature from 1250 to 1350 °C, in agreement with pellet expansion observed in the dilatometry data, Fig. 1(a).

The chemical composition analyses by XRF on the surface of the pellets, Table 1, showed a good agreement between the theoretical and experimental concentration for ceramics sintered at 1250 °C. However, on further increasing the sintering temperature, the concentration of  $\text{TiO}_2$  and  $\text{BaO}$  increased, the concentration of  $\text{SrO}$  remained constant whereas that of  $\text{Bi}_2\text{O}_3$  decreased.

Backscattered SEM images of the cross-section of the pellets were carried out on samples sintered from 1250 °C to

**Fig. 1** (a) Mass loss and linear contraction as function of the temperature. XRD patterns of: (b) powder used to prepare the pellets; pellets sintered at (c) 1150 °C for 6 h and (d) 1300 °C for 2 h



1350 °C. All samples showed the same microstructure; for clarity, we only show data for a pellet sintered at 1250 °C. Two microstructurally- and chemically-distinct regions were observed, Fig. 2. The main phase exhibited small, round grains (not shown) and appeared in whitish tones in the backscatter micrographs whereas the secondary phase exhibited large particles and appeared in blackish tones in the backscatter micrographs, Fig. 3. Mapping images revealed that the main phase contained Ba, Sr, Ti and Bi whereas the secondary phase contained essentially Ba and Ti, Fig. 3. According to the chemical analyses by EDS, the secondary phase appeared to be  $\text{Ba}_4\text{Ti}_{13}\text{O}_{30}$ , a well-known phase present in the  $\text{BaO}$ – $\text{TiO}_2$  system [16]. Since SEM images showed a noticeable presence of secondary phase which was not observed by XRD, these results indicated that the secondary phase appeared to be amorphous.

The estimated grain size of  $(\text{Ba}_{0.6}\text{Sr}_{0.4})_{0.85}\text{Bi}_{0.1}\text{TiO}_3$  by TEM images was in the range  $\sim 0.5$  to  $\sim 2$   $\mu\text{m}$  in the sintering temperature 1250–1350 °C. EDS mapping by TEM on the

$(\text{Ba}_{0.6}\text{Sr}_{0.4})_{0.85}\text{Bi}_{0.1}\text{TiO}_3$  main phase showed that, independently of the sintering temperature, Sr, Ba and Ti were homogeneously distributed through the grains whereas Bi appears to be homogeneously distributed at 1250 °C but, above 1300 °C, evidence of Bi segregation at the grain boundaries was observed, Fig. 4 (regions 3 and 5) and Table 2. In addition, some Al was also present due to the milling media. We note that no Al was detected by XRF since the weak Al peak in the XRF spectrum could not be resolved from that of the Pd XRF source.

Electrical measurements showed that, independently of the sintering temperature, all samples exhibited a similar behaviour. As a representative set, Figs. 5 and 6(a) show the relative permittivity,  $\epsilon_r'$ , and dissipation factor,  $\tan \delta$ , as a function of the temperature as well as the impedance complex plane plot,  $Z''$  vs  $Z'$ , for a pellet sintered at 1350 °C for 2 h.

Thus, above room temperature, the permittivity decreased on increasing temperature and was frequency-independent whereas, below room temperature, it passed through a

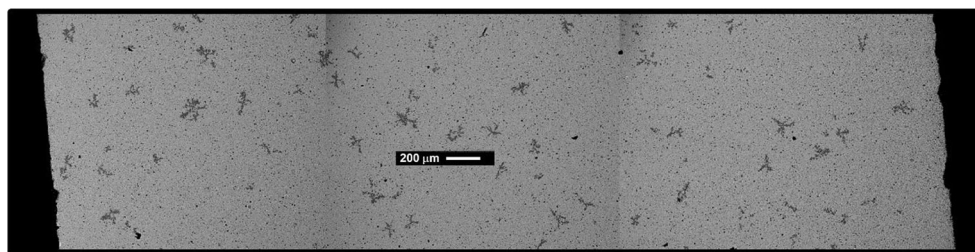
**Table 1** Density, chemical composition,  $\epsilon_r'$ ,  $\tan \delta$  and TTC as function of the sintering temperature

Temp (°C)	Time (h)	Density (%)	Concentration (mass %)†				$\epsilon_r'$	$\tan \delta$ (%)	TCC (ppm/°C)
			BaO	TiO <sub>2</sub>	SrO	Bi <sub>2</sub> O <sub>3</sub>			
1250	2	98.1(2)	35.7(3)	37.6(4)	16.06(5)	10.6(1)	1781(16)	0.07(3)	9.7(5)
1300	2	97.5(2)	36.2(1)	38.1(7)	16.1(1)	9.7(7)	1790(20)	0.05(3)	14.6(6)
1350	2	96.9(3)	36.2(2)	39.3(1)	16.1(3)	9.4(1)	1783(22)	0.05(3)	21(1)

The values and errors represent the average and estimated standard deviation, esd, of three pellets

† Theoretical mass concentration for  $(\text{Ba}_{0.6}\text{Sr}_{0.4})_{0.85}\text{Bi}_{0.1}\text{TiO}_3$ : BaO = 36.10%, TiO<sub>2</sub> = 36.87%, SrO = 16.27% and Bi<sub>2</sub>O<sub>3</sub> = 10.76%

**Fig. 2** Backscattered electron SEM image of the cross section of a pellet sintered at 1250 °C



maximum, was frequency-dependent and showed a relaxor effect, Fig. 5(a). The dissipation factor was frequency-dependent and, at 50 Hz, passed through a minimum over the temperature range -20 °C to 40 °C, Fig. 5(b). Table 1 summarises  $\epsilon_r'$  at 20 °C and  $\tan \delta$  in the temperature range 10 to 30 °C as well as the TCC in the temperature range -25 °C to 100 °C as a function of the sintering temperature. Both  $\epsilon_r'$  and  $\tan \delta$  were approximately independent of the sintering temperature with values around  $\sim 1780$  and  $\sim 0.06\%$ , respectively. By contrast, TCC increased linearly from  $\sim 10 \text{ ppm } ^\circ\text{C}^{-1}$  to  $\sim 21 \text{ ppm } ^\circ\text{C}^{-1}$  on increasing the sintering temperature from 1250 °C to 1350 °C, probably due to an increase in grain size.

In  $Z''$  vs  $Z'$ , Fig. 6(a), each electrically active region of the sample gave rise to a semicircle (ideally) from which the resistance values,  $R$ , were obtained from the intercepts on the  $Z'$  axis whereas the permittivity values were obtained by applying  $2\pi fRC = 1$  at the maximum of each semicircle. Thus,

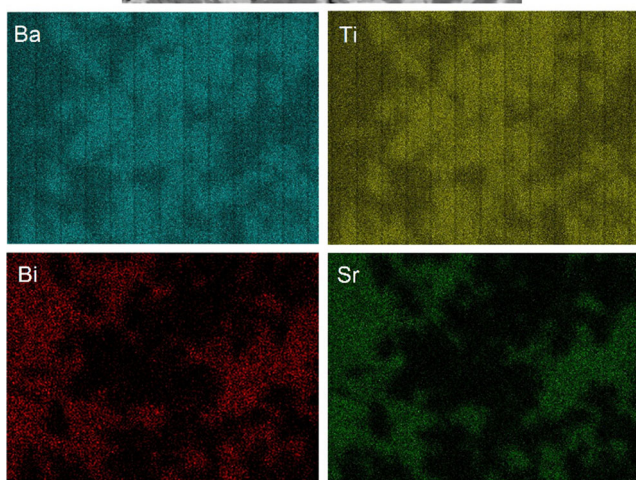
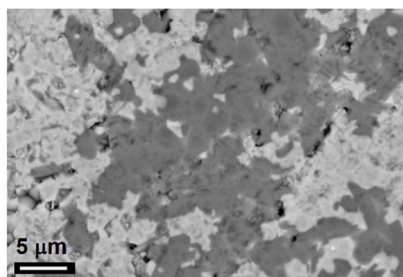


**Fig. 3** Backscatter electron SEM and mapping images of the cross section of a pellet sintered at 1300 °C

independently of the sintering temperature, all samples showed two semicircles from which the resistivity values  $R_1$  and  $R_2$  were obtained. From the magnitudes of the associated permittivity values,  $C_1$  represented the bulk permittivity of the sample, e.g.  $\sim 45 \text{ pF cm}^{-1}$  at  $\sim 350$  °C, whereas  $C_2$  was of the order of nanofarads and was attributed to a grain boundary effect. Bulk and grain boundary conductivity data ( $\sigma = R^{-1}$ ), Fig. 6(b) gave linear Arrhenius plots with similar conductivity and activation energy values independently of the sintering temperature/time. The  $dc$  conductivity at room temperature, extrapolated from the Arrhenius plots, was  $\sim 10^{-20} \text{ S cm}^{-1}$ .

The results presented here show that  $(\text{Ba}_{0.6}\text{Sr}_{0.4})_{0.85}\text{Bi}_{0.1}\text{TiO}_3$  dense ceramics can be obtained in a single-step using stoichiometric amounts of  $\text{BaTiO}_3$ ,  $\text{SrTiO}_3$  and  $\text{Bi}_4\text{Ti}_3\text{O}_{12}$  at

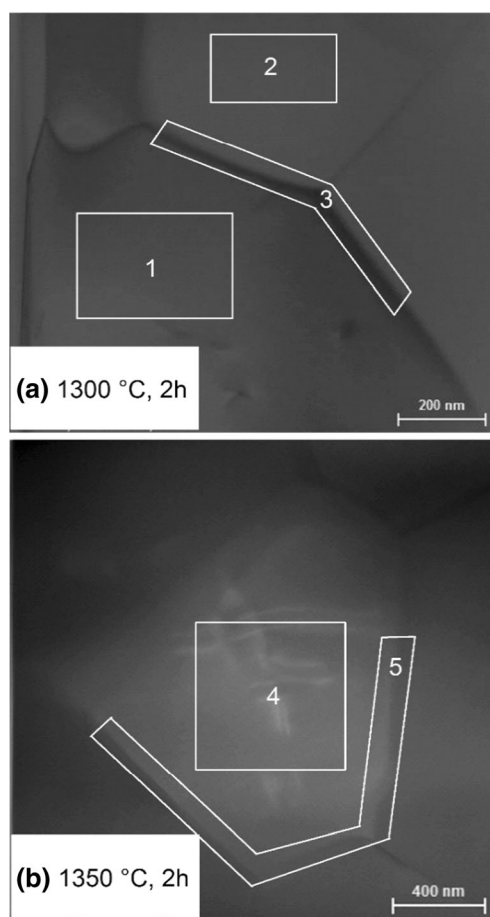


**Fig. 4** Bright field TEM images of ceramics sintered at several temperatures. Areas analysed by EDS are shown

**Table 2** EDS analyses on areas marked in Fig. 4

Area	Element (at.%)				
	Ba	Sr	Bi	Ti	Al
1	33.8	20.4	3.7	40.7	1.4
2	32.9	19.4	4.7	42.1	0.9
3	35.0	17.8	6.3	40.3	0.6
4	25.6	22.0	4.2	46.8	1.4
5	23.1	22.1	5.5	47.7	1.6

temperatures above  $\sim 1250$  °C and sintering times of 2 h.  $\text{Bi}_4\text{Ti}_3\text{O}_{12}$  melts incongruently above  $\sim 1200$  °C (liquidus temperature at  $\sim 1300$  °C) [17–20] and, thus, creates a liquid phase which enhances the reaction. At lower temperatures, where no liquid phase forms, unreacted ceramics are obtained even with sintering times of 6 h, Fig. 1(c, d).

However, the presence of the liquid phase appears to contribute critically to (1) enhance the Bi loss from the ceramic as observed in the TG and XRF data, Fig. 1(a) and Table 1, in particular at temperatures  $\geq 1300$  °C, and (2) promote the formation of a secondary phase, Figs. 2 and 3, although this is often observed in ceramics prepared by liquid-phase/solid-state reactive sintering whose microstructure consists of solid grains and a solidified liquid network [14] or a secondary phase [21].

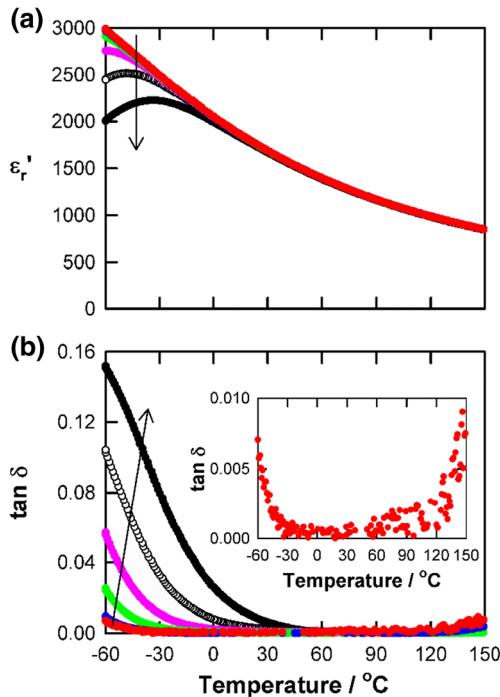


**Fig. 5** (a) Relative permittivity,  $\epsilon_r'$ , and (b) dissipation factor,  $\tan \delta$ , at 50 Hz, 100 Hz, 1 kHz, 10 kHz, 100 kHz and 1 MHz as a function of temperature for a ceramic sintered at 1350 °C. Inset in (b) shows  $\tan \delta$  at 50 Hz. The arrow indicates the direction of increasing frequency from 50 Hz to 1 MHz

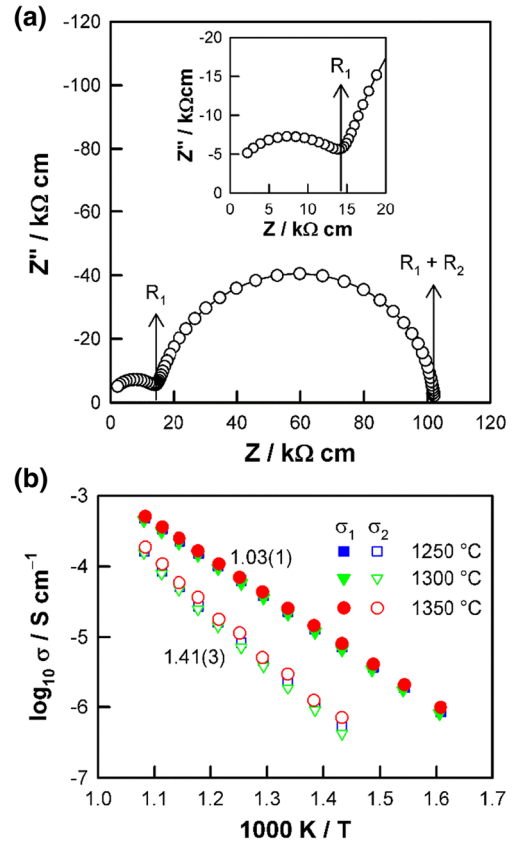


**Fig. 6** (a) Impedance complex plane plot at 525 °C of a ceramic sintered at 1350 °C and (b) Arrhenius plot of bulk,  $\sigma_1$ , and grain boundary,  $\sigma_2$ , conductivity for ceramics sintered at several temperatures. Activation energies, in eV, are noted beside each data set

Nevertheless, neither the secondary phase nor bismuth loss affect the electrical properties. Thus, independently of the sintering temperature,  $(\text{Ba}_{0.6}\text{Sr}_{0.4})_{0.85}\text{Bi}_{0.1}\text{TiO}_3$  ceramics exhibit similar values of relative permittivity, dissipation factor and bulk/grain boundary conductivity, Table 1 and Fig. 6(b), which are comparable to those reported in the literature for the same composition prepared in a two-step process [12]. However, among the sintering temperatures studied here, 1250 °C is the best option from the point of view of energy efficiency during manufacturing. These results should, therefore, be of interest to the ceramics industry.

## 4 Conclusions

$(\text{Ba}_{0.6}\text{Sr}_{0.4})_{0.85}\text{Bi}_{0.1}\text{TiO}_3$  ceramics can be obtained from a mixture of  $\text{BaTiO}_3$ ,  $\text{SrTiO}_3$  and  $\text{Bi}_4\text{Ti}_3\text{O}_{12}$  at 1250 °C with a relative density of  $\sim 98$  %,  $\epsilon_r' \sim 1780$ ,  $\tan \delta \sim 0.07$  % and TTC  $\sim 10$  ppm °C<sup>-1</sup>. However, above that temperature, Bi loss from the ceramic is enhanced. Independently of the sintering temperature,  $(\text{Ba}_{0.6}\text{Sr}_{0.4})_{0.85}\text{Bi}_{0.1}\text{TiO}_3$  ceramics show similar bulk and grain boundary conductivities with an estimated *dc* conductivity at room temperature of  $\sim 10^{-20}$  S cm<sup>-1</sup>.

**Acknowledgements** This work was supported by *Fonds Innovation Recherche du Conseil Départemental des Hautes Pyrénées* [grant number 14051044].

## References

1. M. McQuarrie, *J. Am. Ceram. Soc.* **38**, 444 (1955)
2. J.A. Basmajian, R.C. DeVries, *J. Am. Ceram. Soc.* **40**, 373 (1957)
3. E.N. Bunting, G.R. Shelton, A.S. Creamer, *J. Res. Natl. Bur. Stand.* **38**, 337 (1947)
4. S. Kizaka, S. Ikegami, H. Sasaki, *J. Phys. Soc. Jpn.* **14**, 1680 (1959)
5. B. Jaffé, W. R. Cook Jr and H. Jaffé, in *Piezoelectric Ceramics*, ed. By J. P. Roberts and P. Popper (Academic Press, London, 1971) ch. 3, pp. 53
6. V.V. Lemanov, E.P. Smirnova, P.P. Syrnikov, E.A. Tarakanov, *Phys. Rev. B* **54**, 3151 (1996)
7. L. Zhou, P.M. Vilarinho, J.L. Baptista, *J. Eur. Ceram. Soc.* **19**, 2015 (1999)
8. L. Zhou, P.M. Vilarinho, J.L. Baptista, *Bol. Soc. Esp. Ceram. V.* **38**, 599 (1999)
9. L. Zhou, P.M. Vilarinho, J.L. Baptista, *J. Electroceram.* **5**, 191 (2000)
10. L. Zhou, P.M. Vilarinho, J.L. Baptista, *J. Eur. Ceram. Soc.* **21**, 531 (2001)
11. W. Chen, X. Yao, X. Wei, *Solid State Commun.* **141**, 84 (2007)
12. W. Chen, X. Yao, X. Wei, *J. Mater. Sci.* **43**, 1144 (2008)
13. F. Bahri, H. Khemakhem, *Ceram. Int.* **39**, 7571 (2013)
14. R.M. German, P. Suri, S.J. Park, *J. Mater. Sci.* **44**, 1 (2009)
15. J. Tong, D. Clark, M. Hoban, R. O'Hayre, *Solid State Ionics* **181**, 496 (2010)
16. N. Zhu, A.R. West, *J. Am. Ceram. Soc.* **93**, 295 (2010)
17. E.I. Speranskaya, I.S. Rez, L.V. Kozlova, V.M. Skorikov, V.I. Slavov, *Izv. Akad. Nauk SSSR Neorg. Mater.* **1**, 232 (1965)
18. J.R. Esquivel Elizondo, B.B. Hinojosa, J.C. Nino, *Chem. Mater.* **23**, 4965 (2011)
19. J. Lopez Martinez, A. Romero Serrano, A. Hernandez Ramirez, B. Zeifert, C. Gomez Yañez, R. Martinez Sanchez, *Thermochim. Acta* **16**, 35 (2011)
20. Y.F. Kargin, S.N. Ivicheva, V.V. Volkov, *Russ. J. Inorg. Chem.* **60**, 619 (2015)
21. D.R. Clarke, *J. Am. Ceram. Soc.* **82**, 485 (1999)